Climate Dynamics (2018) 51:2127–2140
https://doi.org/10.1007/s00382-017-4003-4

The influence of ENSO, PDO and PNA on secular rainfall variations in Hawai'i

Abby G. Frazier[1] · **Oliver Elison Timm**[2] · **Thomas W. Giambelluca**[3] · **Henry F. Diaz**[3]

Received: 19 July 2017 / Accepted: 6 November 2017 / Published online: 16 November 2017

Abstract
Over the last century, significant declines in rainfall across the state of Hawai'i have been observed, and it is unknown whether these declines are due to natural variations in climate, or manifestations of human-induced climate change. Here, a statistical analysis of the observed rainfall variability was applied as first step towards better understanding causes for these long-term trends. Gridded seasonal rainfall from 1920 to 2012 is used to perform an empirical orthogonal function (EOF) analysis. The leading EOF components are correlated with three indices of natural climate variations (El Niño-Southern Oscillation (ENSO), Pacific Decadal Oscillation (PDO), and Pacific North American (PNA)), and multiple linear regression (MLR) is used to model the leading components with climate indices. PNA is the dominant mode of wet season (November–April) variability, while ENSO is most significant in the dry season (May–October). To assess whether there is an anthropogenic influence on rainfall, two methods are used: a linear trend term is included in the MLR, and pattern correlation coefficients (PCC) are calculated between recent rainfall trends and future changes in rainfall projected by downscaling methods. PCC results indicate that recent observed rainfall trends in the wet season are positively correlated with future expected changes in rainfall, while dry season PCC results do not show a clear pattern. The MLR results, however, show that the trend term adds significantly to model skill only in the dry season. Overall, MLR and PCC results give weak and inconclusive evidence for detection of anthropogenic signals in the observed rainfall trends.

Keywords Rainfall · Hawai'i · EOF analysis · Attribution · ENSO · PDO

1 Introduction

Recent evidence indicates that rainfall in Hawai'i has been trending downward since 1920. Consecutive dry days (days with no rainfall) have increased on all islands since the 1950s (Chu et al. 2010; Kruk et al. 2015). At high elevations, seasonal drying trends have been detected (Longman et al. 2015) and are already having impacts on ecosystems (Krushelnycky et al. 2013, 2016). A recent spatial trend analysis showed that for the period 1920 to 2012, over 90% of the State experienced drying trends (Fig. 1), although running trend analysis showed that many trends were statistically significant only during certain time periods, and short-term trends (20–30 years) experienced regular oscillations in the sign of the trend (Frazier and Giambelluca 2017). Some of this drying in the wet season since the 1950s has been associated with reduced rainfall during La Niña years (O'Connor et al. 2015). Rainfall in Hawai'i is strongly influenced by large-scale modes of climate variability, particularly, the El Niño-Southern Oscillation (ENSO), the Pacific Decadal Oscillation (PDO), and the Pacific North American (PNA) (Lyons 1982; Chu et al. 1993; Chu and Chen 2005; Elison Timm et al. 2011). However, it is unknown how much of the apparent declines in rainfall are due to natural variations in climate or anthropogenic effects. Identifying the drivers of these trends is important to understand current rainfall variability and to predict future rainfall changes in Hawai'i.

Electronic supplementary material The online version of this article (https://doi.org/10.1007/s00382-017-4003-4) contains supplementary material, which is available to authorized users.

✉ Abby G. Frazier
abbyfrazier@fs.fed.us

[1] Institute of Pacific Islands Forestry, USDA Forest Service, 60 Nowelo Street, Hilo, HI 96720, USA

[2] Department of Atmospheric and Environmental Sciences, State University of New York at Albany, Albany, NY, USA

[3] Department of Geography, University of Hawai'i at Mānoa, Honolulu, HI, USA

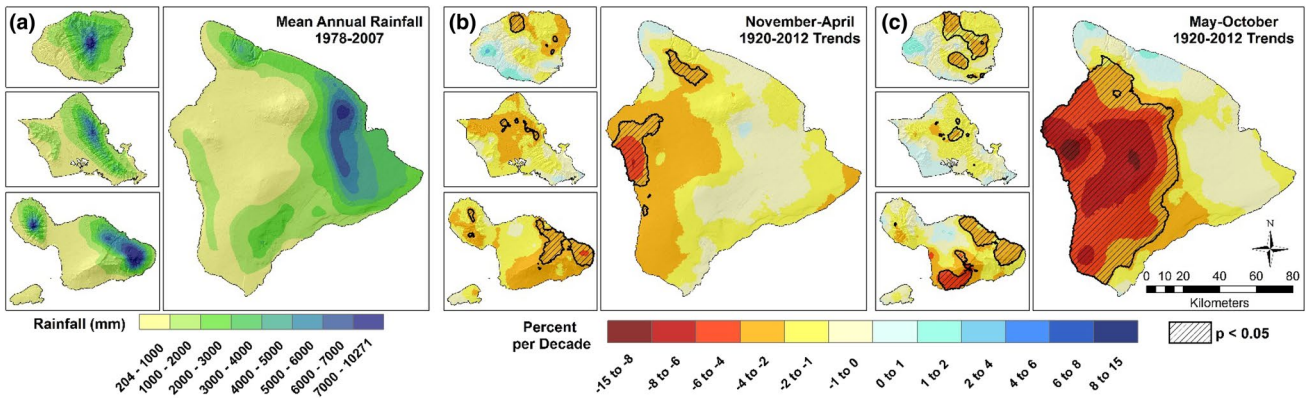

Fig. 1 Mean annual rainfall in millimeters (**a**) from 1978 to 2007 (adapted from Giambelluca et al. 2013), and season rainfall trend maps in percent per decade from 1920 to 2012 (adapted from Frazier and Giambelluca 2017) for wet season (November–April, **b**) and dry season (May–October, **c**); significant trends ($p < 0.05$) are indicated with black hatching. All maps shown on same spatial scale for the four major islands considered in this study: Kaua'i, O'ahu, Maui, and Hawai'i Island

Anthropogenic influence on global precipitation, beyond changes explained by internal climate variability, has been detected (Zhang et al. 2007; Noake et al. 2012). Many regional-scale studies, however, have not detected an anthropogenic signal in rainfall trends above the noise of natural variability (Hoerling et al. 2006; Wang et al. 2009; Sarojini et al. 2016). Attribution studies seek to determine whether certain external drivers are the cause of the observed change for a given variable. A common approach is to simulate the variable in climate models both with and without anthropogenic forcing and to compare observations with the model simulations to detect anthropogenic signals (Stott et al. 2010). However, at small spatial scales (e.g., < 2000 km), the signal-to-noise ratio decreases making it more difficult to detect significant changes (Stott and Tett 1998), and models may not adequately capture external forcings or internal variability at these regional scales (Hegerl and Zwiers 2011). Thus, many regional attribution studies focus on quantifying only the influences of natural climate variability on rainfall using empirical methods (L'Heureux 2004; Ashcroft et al. 2014; Xiao et al. 2015). Quantifying the amount of anthropogenic influence on climatic trends is difficult, and most studies attempt to remove the contribution from internal climate variability, and determine if a significant trend remains (Hamlington et al. 2013)—however, it might still be difficult to prove that the trend is anthropogenically driven. Methods often used to determine the influence of natural climate variability include simple correlation analysis (Silvestri and Vera 2003), empirical orthogonal function (EOF) analysis or singular value decomposition analysis (Taschetto and England 2009; Ummenhofer et al. 2009; Feng and Li 2011; Elsanabary et al. 2014; Ning and Bradley 2014; Kim and Ha 2015; Xiao et al. 2015), multiple linear regression (L'Heureux 2004; Kolker and Hameed 2007; Ashcroft et al. 2014; Chylek et al. 2014; Ning and Bradley 2014), and climate model simulations (Wang et al. 2009; Meyssignac et al. 2012).

The spatial extent of the main Hawaiian Islands (~500 km wide) is small compared to climate model grid cells (typically 100 km horizontal grid spacing or greater). Climate patterns in Hawai'i are characterized by exceptionally high spatial variability, and the complex terrain-influenced processes which operate on relatively small spatial scales are not well represented by the coarse-resolution global climate models (GCMs) (Elison Timm et al. 2015); the major Hawaiian Islands may be represented by only a few grid cells in a GCM (Lauer et al. 2013). Both statistical downscaling (SDS) and dynamical downscaling (DDS) methods have been used for Hawaiian rainfall to relate information from global-scale models to the regional scale (less than 3 km horizontal grid spacing) (Lauer et al. 2013; Elison Timm et al. 2015; Zhang et al. 2016a, b). The latest statewide DDS rainfall results use the A1B scenario from CMIP3 global model projections for 2080–2099, and the SDS results use the RCP8.5 scenario from CMIP5 projections for 2071–2100. SDS end of century results for the wet season (Fig. 2a) indicate a strong dipole structure between windward and leeward areas, where leeward areas exhibit strong drying trends and windward slopes become wetter or remain stable (Elison Timm et al. 2015). The dry season results indicate strong drying across most islands in the leeward (arid/semiarid) areas, with no strong trends along the wet windward regions (Fig. 2b). DDS results for the wet season (Fig. 2c) are similar to the SDS results in that they also show a dipole structure, but find only modest drying trends in leeward areas (Zhang et al. 2016a, b). The dry season DDS projections (Fig. 2d) are quite different from the SDS results, showing a strong dipole pattern with windward areas projected to experience increases in rainfall up to 65% and modest drying in leeward areas. The discrepancies in the sign and magnitude of future changes

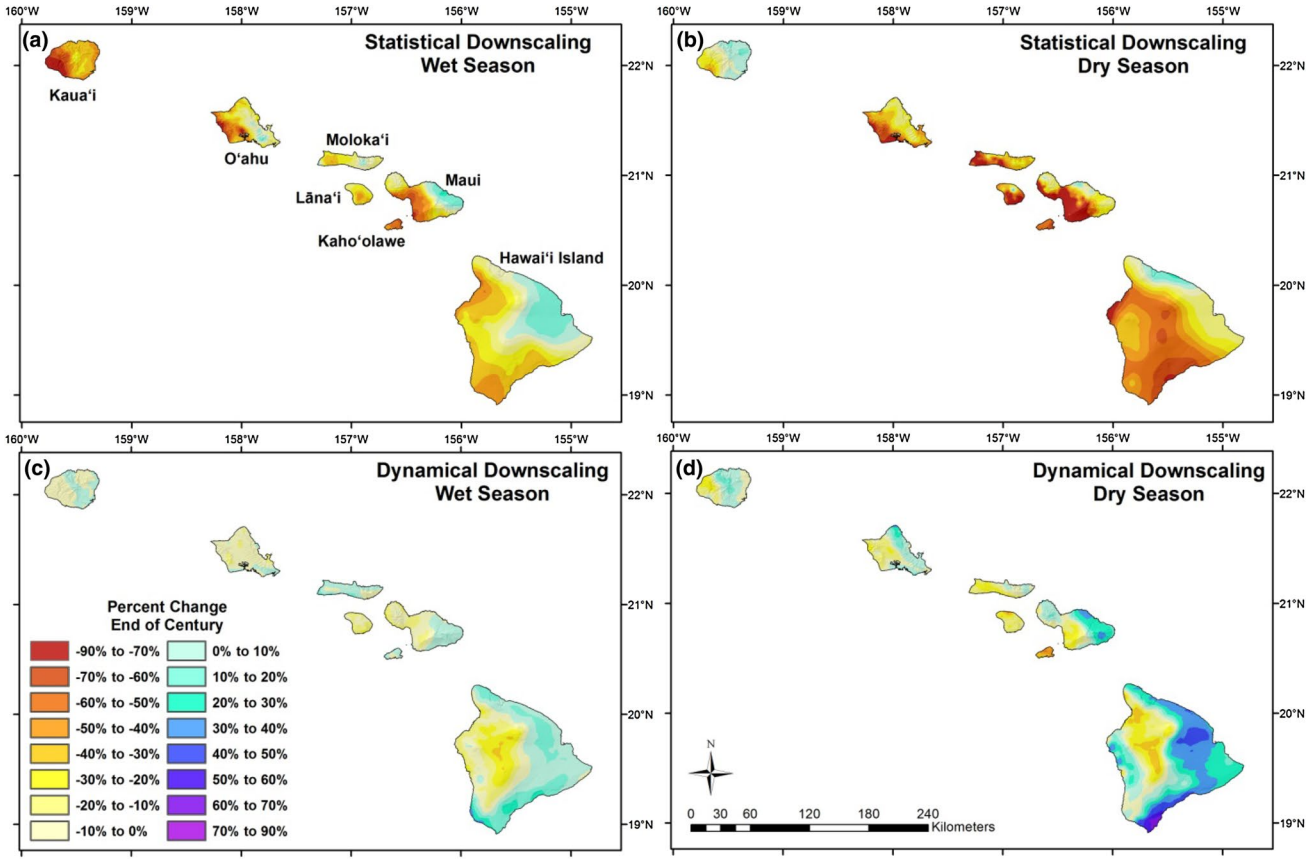

Fig. 2 Percent change in seasonal rainfall at the end of the century for the State of Hawai'i as projected by statistical downscaling (Elison Timm et al. 2015) for 2071–2100, relative to the 1978–2007 seasonal mean for wet season (Nov.–Apr.) (**a**) and dry season (May–Oct.) (**b**) and dynamical downscaling (Zhang et al. 2016a, b) for 2080–2099 relative to the modeled 1990–2009 seasonal mean for wet season (**c**) and dry season (**d**)

between these approaches, especially in the dry season, are not only indicative of the differences in methodologies and model/scenario choices, but are thought to be representative of the generally high uncertainty surrounding future projections of rainfall in Hawai'i.

Here, our objectives are to quantify the total contribution of natural climate variability to seasonal rainfall variations over the period of record, and to assess whether an anthropogenic signal can be detected above what can be explained by natural variability. The influence of natural and anthropogenic factors on rainfall was assessed by performing an empirical orthogonal function (EOF) analysis to determine the leading modes of variability for rainfall in Hawai'i. Following L'Heureux (2004) and others, we correlated the leading components with the dominant modes of natural climate variability, and the relative influence of each was determined through multiple linear regression (MLR). Pattern correlation coefficients [PCC, (Bhend and von Storch 2008)] were also calculated between the observed rainfall trends and the future change in rainfall from downscaling outputs to assess whether the most recent trends are consistent with what the models project in response to climate change, which we could interpret as evidence of an anthropogenic signal that has emerged in observed trends. By combining the strength of several methods, we can better understand what is driving current rainfall trends in Hawai'i, and this information can aid managers in preparing for future climatic variations.

2 Study area and data

2.1 Study area

The State of Hawai'i is located in the Pacific Ocean between 18.9° and 22.24°N latitude and 160.25° and 154.8°W longitude with a total land area of 16,637 km^2 (Juvik and Juvik 1998). Climate patterns are extremely diverse due in large part to the complex topography, with mean annual rainfall ranging (Fig. 1a) from ~200 mm to over 10,000 mm (Giambelluca et al. 2013). Most areas in the state experience a wet season in winter (November – April) and a dry season in summer (May–October). The prevailing winds are northeast

trade winds, and much of the rainfall is orographic, resulting in wet windward areas and dry leeward areas. Hawai'i also has a trade wind inversion layer at around 2200 m (Cao et al. 2007; Longman et al. 2015), leading to very dry areas above this elevation. This study will focus on the four largest Hawaiian Islands: Kaua'i, O'ahu, Maui, and Hawai'i Island.

2.2 Large-scale climate variability

Modes of large-scale climate variability in the Pacific have strong influences on Hawai'i's weather and climate. ENSO is associated with changes in the strength of the Hadley Cell circulation and its dominant signals are in the tropical Pacific. The phases recur every 3–7 years, and persist for 6 to 18 months. The warm phase of ENSO (El Niño) generates dry winter (wet season) conditions in Hawai'i, while the cool phase (La Niña) leads to wetter winter conditions (Chu and Chen 2005; Diaz and Giambelluca 2012) – although the positive rainfall anomalies experienced during La Niña have been declining over the past few decades (O'Connor et al. 2015). The dominant signals of the PDO are found in the northern Pacific, with secondary signals in the tropics, and PDO phases have significant impacts on rainfall in Hawai'i (Chu and Chen 2005; Diaz and Giambelluca 2012). Despite the PDO being a complex chain of interactions in the climate system (Newman et al. 2016) a key signature of the PDO is a similar spatial sea surface temperature (SST) anomaly pattern as ENSO; however, each phase can persist for 20–30 years (Mantua et al. 1997; Mantua and Hare 2002). Hawaiian rainfall is negatively correlated with the PDO index, and when El Niño = events occur during positive PDO phases, the rainfall response is enhanced (Chu and Chen 2005). PNA is a dominant mode of variability in the North Pacific extratropical atmosphere, with variability on interannual and decadal time scales (Wallace and Gutzler 1981). The signals appear in all months except June and July. The negative PNA phase is associated with below-average 500 hPa geopotential heights over Hawai'i and Western Canada/US, and with above average heights over the Aleutian Islands and the Eastern US The positive phase shows the opposite pattern, with above-average heights near Hawai'i, which produces drier conditions for the State. The interactions between tropical climate variability and extratropical climate on interannual and decadal time scales are not fully understood. However, the physical interactions lead to a pronounced co-variability among ENSO, PNA and PDO climate indices, which limits the ability to attribute regional rainfall variability to a single climate mode.

3 Data

This study utilizes high resolution (250 m) gridded monthly and annual rainfall from 1920 to 2012 (Frazier et al. 2016). After performing a geostatistical method comparison between three kriging methods and two covariates, ordinary kriging was used to interpolate monthly relative anomalies (monthly rainfall/mean monthly rainfall) relative to the 1978–2007 monthly mean (Giambelluca et al. 2013) from over 1000 rain gauge stations. The anomaly maps were multiplied by the mean maps to produce the final monthly and annual maps. Prior to interpolation, the rain gauge data were subjected to statistical quality control measures, homogeneity tests, and gap filling procedures. For complete details, see Giambelluca et al. (2013) and Frazier et al. (2016). For this study, seasonal rainfall maps were derived from the monthly data set.

The index used to represent the strength and phase of ENSO is the Multivariate ENSO Index (MEI) (Wolter and Timlin 2011). This index is derived from six variables over the tropical Pacific: sea-level pressure, meridional surface wind, zonal surface wind, surface air temperature, sea surface temperature, and total cloudiness fraction. The MEI was chosen because it incorporates more information from the atmosphere and ocean into a single index than indices focused on either ocean SSTs (e.g., NINO3.4 index) or atmospheric pressure fields (e.g., Southern Oscillation Index). The multivariate information is expected to better represent the atmospheric state over the Hawaiian Islands. The PDO index (PDOI) is the standard index used for this mode of variability, and is calculated as the first principal component of the North Pacific monthly sea surface temperature (Mantua et al. 1997; Mantua and Hare 2002). The PNA index (PNAI) is calculated by projecting the PNA loading pattern onto the daily anomaly 500 hPa height field in the Northern Hemisphere (Barnston and Livezey 1987; Van Den Dool et al. 2000; Chen and Van den Dool 2003). The PNAI is only available starting in 1950, so all analyses involving PNAI in this study will be for the period 1950–2012. Time series of the three climate indices for both seasons are given in Fig. 3, along with average statewide rainfall over the same period (derived from Frazier et al. 2016).

4 Methods

4.1 Empirical orthogonal function analysis

A common statistical technique used to analyze variability in rainfall time series is an empirical orthogonal function (EOF) analysis. The purpose of EOF analysis is to decompose a continuous space–time field into a new, smaller set of

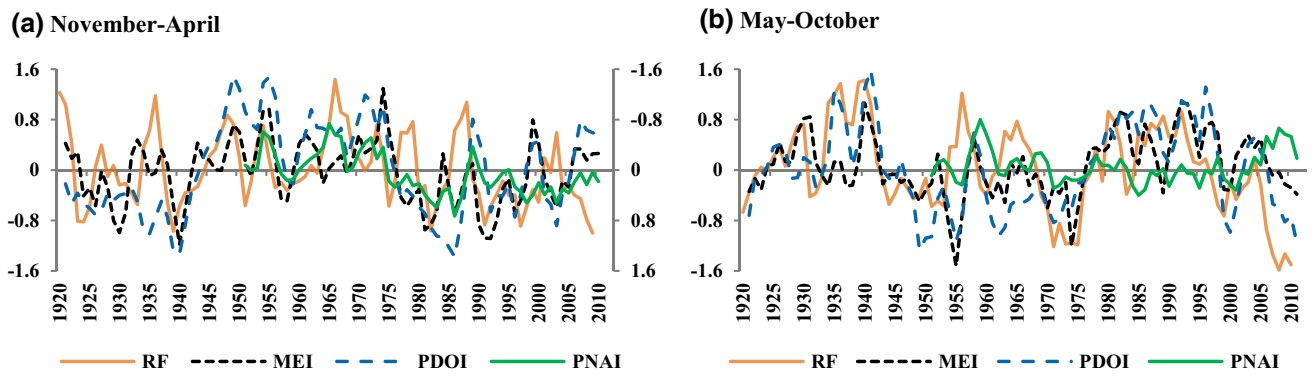

Fig. 3 Time series of MEI, PDOI, PNAI, and statewide average rainfall (RF) time series for November to April (**a**) and May–October (**b**). All time series are 3-year running means, and the rainfall is standardized. The three climate indices (MEI, PDOI, and PNAI) in November–April (**a**) are plotted on the secondary y-axis in reverse order. The PNAI time series starts in 1950

variables that capture most of the original variance through linear combinations of the original variables. EOF is used to condense a large time series dataset into a smaller dataset representative of the original variability; the first few components account for most of the original variability. A previous study in Hawai'i by Lyons (1982) used a subset of 63 rainfall stations and performed an EOF analysis for a 37-year period (1939–1975). In that study, the first three components accounted for 73% of the variance and each spatial pattern had an apparent relationship to physical rainfall-producing processes: trade wind orographic rainfall, southwest wind orographic rainfall, and convective rainfall patterns. Here, we applied EOF analysis to the gridded rainfall dataset (284,408 pixels) and to station data for the four major islands (Kaua'i, O'ahu, Maui and Hawai'i Island) and two seasons: November–April and May–October. The leading components were then correlated with the three indices of large-scale modes of climate variability (MEI, PDOI, and PNAI), and the spatial patterns of the loadings from the EOF analysis were related to physical processes if possible. A correlation analysis was also performed between the raw rainfall time series and each of the climate indices at every 250 m pixel for each of four seasons. The Pearson correlation and significance values between the rainfall values and each climate index were then mapped to show spatial patterns of the relationships between seasonal rainfall and large-scale modes of climate variability.

4.2 Multiple linear regression

Multiple Linear Regression (MLR) was used to model the leading EOF components as a combination of the three climate indices, representing natural climate variability, and a trend index time series to represent anthropogenic influence. Two options were tested for the trend term: a global temperature anomaly time series (obtained via the National Climatic Data Center, http://www.ncdc.noaa.gov/cag/time-series/global) and a linear trend. Variance inflation factors (VIF) were used to detect multicollinearity since the three climate indices are not independent of each other. Additive and full models (with all interactions) were considered, and type II ANOVA and R^2 results were used to compare models. To calculate the total amount of rainfall variability explained by these factors, the R^2 values from each MLR model were multiplied by the percent variability that each EOF component represents.

4.3 Pattern correlations

To determine the similarity between the most recent rainfall trends and the future response to climate change projected from downscaling products (expected trends), the pattern correlation coefficient (PCC) was calculated (Bhend and von Storch 2008). The PCC compares dimensionless patterns of recent (R) and expected (E) trends: $R^* = \frac{R}{\|R\|}$ and $E^* = \frac{E}{\|E\|}$, where $\|R\|$ and $\|E\|$ are defined as:

$$\|R\| = \sqrt{\frac{1}{n}\sum_{i=1}^{n} R_i^2} \quad \|E\| = \sqrt{\frac{1}{n}\sum_{i=1}^{n} E_i^2}, \tag{1}$$

where i counts the spatial pixels $i = 1, \ldots, n$. The PCC is then calculated from the following:

$$PCC = \frac{1}{n}\sum_{i=1}^{n} R_i^* E_i^* = \frac{\sum_{i=1}^{n} R_i E_i}{\sqrt{\sum_{i=1}^{n} R_i^2 \sum_{i=1}^{n} E_i^2}}, \tag{2}$$

where $-1 \le PCC \le 1$. Note that the PCC takes into account the average values of R_i and E_i. To represent the expected trends (E), the most recent statistical and dynamical downscaling percent change results were used for the end of

century in the wet and dry seasons (Fig. 2) (Elison Timm et al. 2015; Zhang et al. 2016a, b). SDS and DDS projections were resampled from 3 km to 250 m resolution for comparison with recent rainfall trends. The SDS results show that the spatial structure of the anomaly patterns is not sensitive to the chosen RCP or the selected time interval, only the amplitude changes significantly. Percent change for SDS is calculated relative to the 1978–2007 Rainfall Atlas of Hawai'i seasonal mean maps (Giambelluca et al. 2013), while the future percent change for DDS is calculated relative to the modeled present day (1990–2009) seasonal means (Zhang et al. 2016a). For the recent trends (R), every possible overlapping trend map is used (where trend period includes at least 20 years) between 1920 and 2012 (Frazier and Giambelluca 2017). Using gridded seasonal rainfall data, linear trends were calculated at every 250 m pixel for each combination of start year and trend period, producing 2775 trend maps in each season. To display the results, we use a plot similar to the running trend plots from Frazier and Giambelluca (2017) and Brunetti et al. (2012), where the start year of the recent trend map is plotted on the x-axis, and the end year of the recent trend is on the y-axis. The color of the point represents the value of the PCC between each recent rainfall trend map and the future expected change from the downscaling maps.

5 Results

5.1 Correlation and EOF analysis

The correlation maps between the rainfall time series and the MEI, PDOI, and PNAI at each pixel (Figs. 4, 5) show that all indices are negatively correlated with rainfall in winter, and have positive or near zero correlation in summer. PNAI has stronger correlations with rainfall than MEI and PDOI in the wet season, and almost no correlation with rainfall in the dry season, which is not surprising as the PNA teleconnection

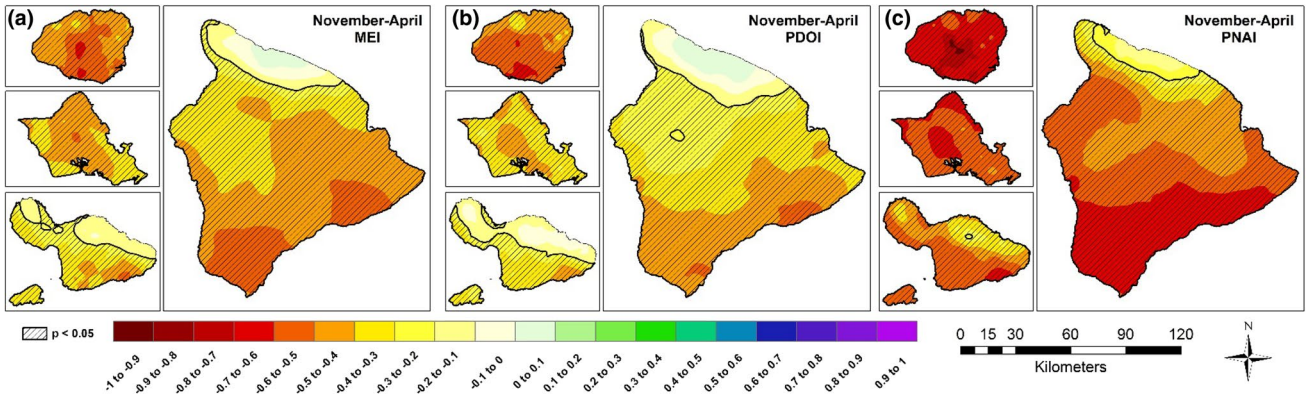

Fig. 4 November to April seasonal rainfall correlations with three climate indices: MEI (**a**), PDOI (**b**), and PNAI (**c**) for the four major islands from 1920 to 2012, except PNAI which is from 1950 to 2012. Statistically significant trends ($p < 0.05$) are indicated with black hatching

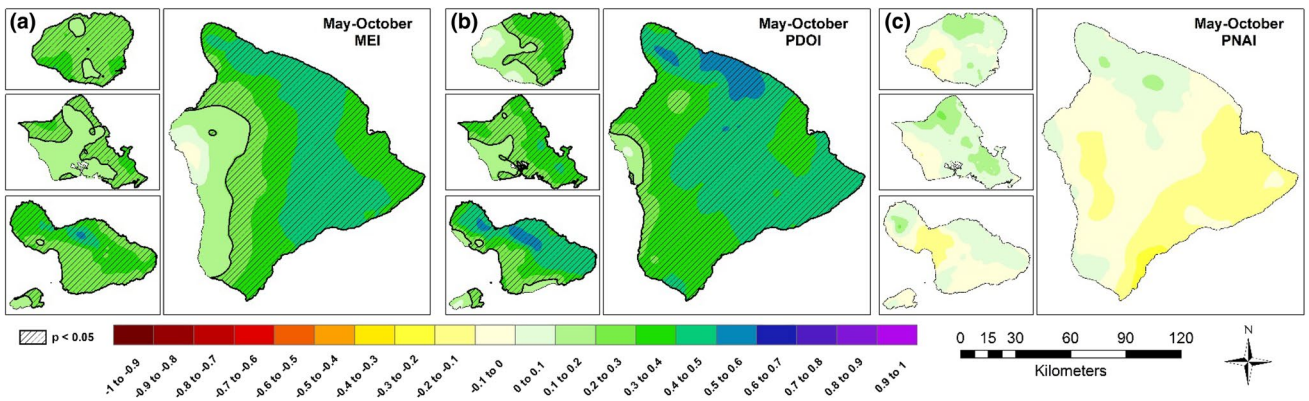

Fig. 5 May to October seasonal rainfall correlations with three climate indices: MEI (**a**), PDOI (**b**), and PNAI (**c**) for the four major islands from 1920 to 2012, except PNAI which is from 1950 to 2012. Statistically significant trends ($p < 0.05$) are indicated with black hatching

is weaker in general and does not influence the subtropical Pacific in the summer months. Kaua'i and O'ahu have slightly higher wet season correlations with the PNAI than Maui or Hawai'i Island. The correlation patterns for rainfall vs. MEI and rainfall vs. PDOI are very similar in the two seasons, and for both MEI and PDOI, the windward areas of Maui and Hawai'i Islands have no significant correlations in the wet season. In the dry season, the southern islands (Maui and Hawai'i Island) have much higher correlations than the northern islands (Kaua'i and O'ahu), particularly in windward areas, while leeward areas tend to have lower correlations. This can be explained by the fact that the leeward areas experience a few rainfall events through small scale or mesoscale disturbances. Summer seasonal average circulation indices are not sensitive metrics for such precipitation regimes.

From the EOF analysis we examined the percent of the variability explained by the leading components (Fig. 6; Online Resource 1) from EOF analysis on station data (Station EOF) and on the gridded rainfall data (Grid EOF). For both analyses (Station and Grid), the majority of the variability is captured by the first component, and the following components have much smaller contributions to the total variability. In the Grid EOF, more variability is captured by the first component in wet season (81% on average) than dry season (72% on average). In the wet season, all islands have at least 74% variability captured by the first component, while in the dry season, only one island (O'ahu) had more than 73% variability explained by the first component. The northern islands have more variability explained than southern islands in E1, while E2 captures more variability on the southern islands. One known problem with EOF analysis is to identify the number at which the EOF patterns can and should be analyzed and associated with physical mechanisms. Here, we make use of North's rule of thumb (North et al. 1982; Hannachi et al. 2007). As can be seen in Online Resource 1, the error bars in the eigenvalues overlap between EOF modes 3 and 4 for most islands and seasons, but not all (e.g., Hawai'i Island, Nov.-Apr.). For Hawai'i Island, including E3 adds up to 7.4% variability. Taken together, both the amount of explained variance and the statistical selection rule of thumb, it was decided to concentrate the remainder of the analysis and discussion on the EOF modes 1–3. Therefore, all presented results use the top three components (E1-E3), representing a total of 84–95% of the variability in the rainfall time series.

The spatial patterns of the loadings for the Grid EOF were very similar for both seasons. The patterns for the wet season (Fig. 7) and dry season (Fig. 8) show a monopole structure in the first component (E1), while all other components exhibit a dipole structure. As expected due to the relatively high fraction of variance explain by the first EOF, the time series for E1 aligns almost perfectly with the statewide average rainfall in both seasons (Figs. 7d, 8d). The second component (E2) appears to represent a trade wind (orographic) regime, where peak values are seen over windward areas, similar to the mean annual rainfall patterns (Fig. 1a). The time series for E2 captures the seesaw pattern associated with strong windward-leeward variability, where years with a wet windward and dry leeward pattern have high PC scores, and years where leeward areas experienced wetter conditions correspond with drier than normal windward areas. The third component (E3) does not appear to represent a physical rain-producing mechanism, thus supporting the North's selection rule; it is likely that E3 is a combination of the true (but unknown) EOF modes. The orthogonality constraints of the EOF analysis can produce spatial patterns that are a mixture of different physical mechanisms, and therefore make physical interpretation difficult (Hannachi et al. 2007; Ning and Bradley 2014).

We also compared the EOF eigenvalue spectrums and the associated spatial patterns between Station EOF and Grid EOF. The first components from the Grid EOF explain more variability than the first components in Station EOF (especially on Hawai'i Island; in the wet season, 74% variability is explained by E1 in Grid EOF, 56% in Station EOF, Fig. 6). Because the high resolution grids were derived from the station data through spatial interpolation, we would expect a larger fraction of explained variability in the gridded data. When the spatial loading patterns of Station EOF (not

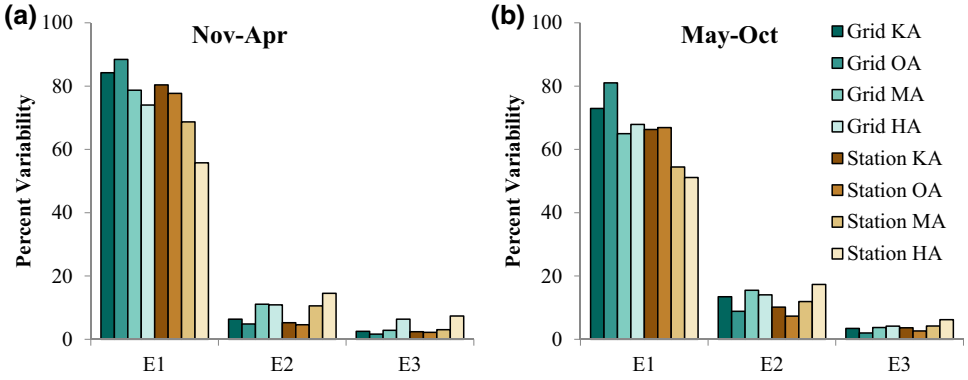

Fig. 6 Percent variability explained by the top three EOF components (E1–E3) by island for Grid EOF and Station EOF for two seasons: November–April (**a**) and May–October (**b**). *KA* Kaua'i, *OA* O'ahu, *MA* Maui, *HA* Hawai'i Island

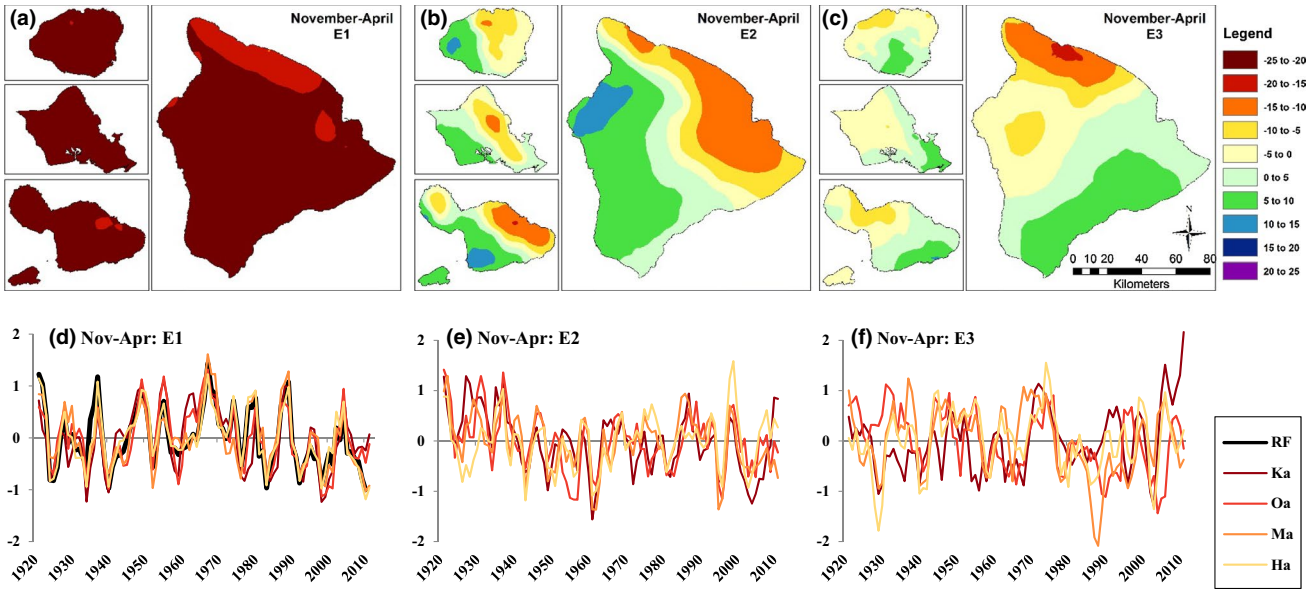

Fig. 7 November to April EOF patterns of the leading three EOF components (**a–c**) (units: millimeters per standard deviation) and the standardized 3-year running mean time series (**d–f**) for the four major islands shown for the Grid EOF analysis. Panel (**d**) also includes the standardized statewide 3-year running mean rainfall time series from November–April in black (Frazier et al. 2016). *Ka* Kaua'i, *Oa* O'ahu, *Ma* Maui, *Ha* Hawaii Island

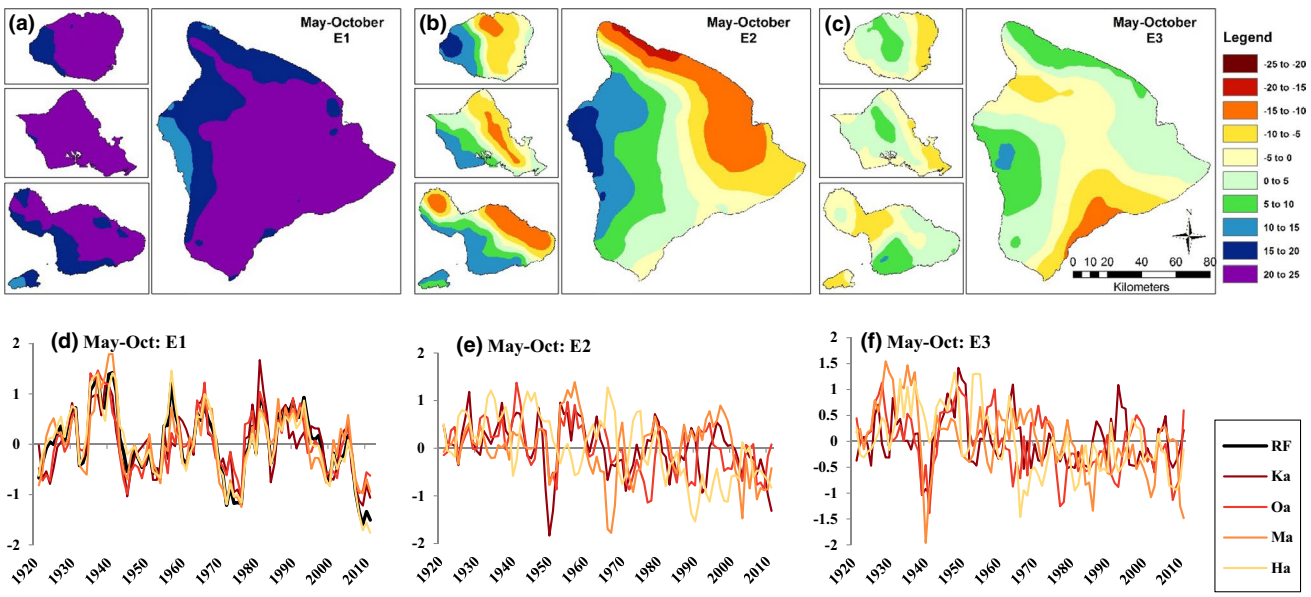

Fig. 8 May to October EOF patterns of the leading three EOF components (**a–c**) (units: millimeters per standard deviation) and the standardized 3-year running mean time series (**d–f**) for the four major islands shown for the Grid EOF analysis. Panel (**d**) also includes the standardized statewide 3-year running mean rainfall time series from May–October in black (Frazier et al. 2016). *Ka* Kaua'i, *Oa* O'ahu, *Ma* Maui, *Ha* Hawai'i Island

shown) and Grid EOF (Figs. 7, 8) are compared, the patterns show very similar results, indicating that the spatial results from this study do not depend on whether station data or gridded data are used.

The EOFs were correlated with the three climate indices, and results (Fig. 9) show that the highest correlations are between E1 and PNAI in the wet season. Correlations with MEI and with PDOI are similar to each other in both seasons for all three EOFs, with the smallest correlations in E2.

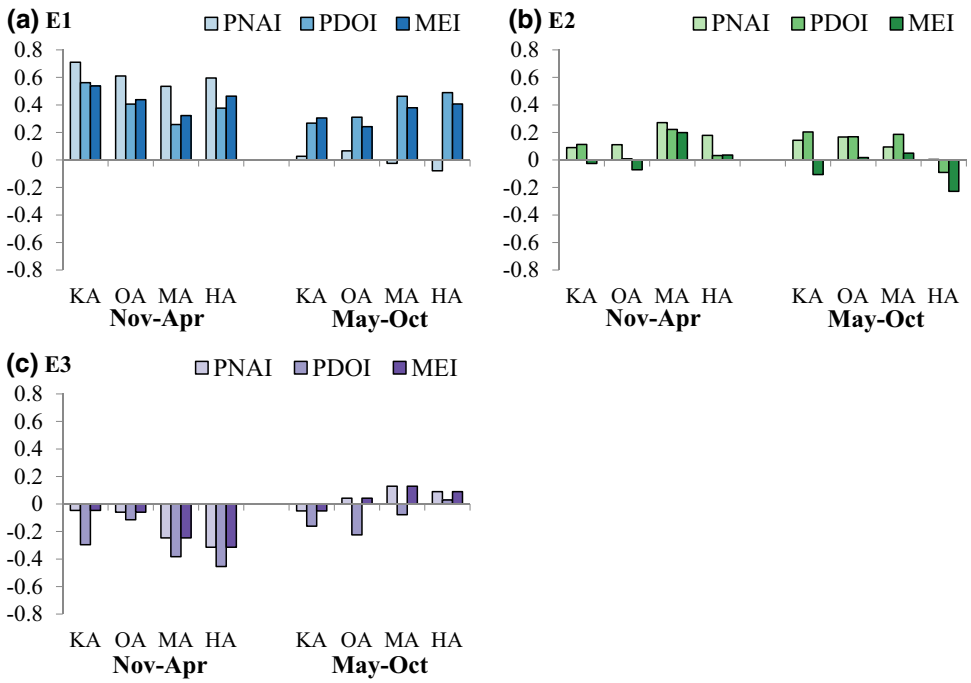

Fig. 9 Correlations between the three indices (MEI, PDOI, PNAI) and the leading three EOF components (E1–E3) (**a**–**c**), by island and two seasons (November–April and May–October). *KA* Kaua'i, *OA* O'ahu, *MA* Maui, *HA* Hawai'i Island

We note here that the three indices, in particular the PDO index during the wet season, exhibits negative correlations with E3. This result highlights that the spatiotemporal rainfall variability is responding on different time scales with a somewhat different spatial rainfall anomaly pattern. In the next section, we address the extent to which the leading EOF modes can be explained by a linear combination of the three climate indices, and if a secular trends can be associated with the EOF modes.

5.2 Multiple linear regression with climate indices

MLR was used with the standardized climate indices (MEI, PDOI and PNAI) and a trend term as predictors of the standardized EOF time series. VIF results did not detect serious multicollinearity between the climate indices; average VIF values were <2, with maximum VIF = 2.38. The two datasets used to represent the "trend" term in the model (global temperature and a linear trend), behaved similarly and produced very similar results (Online Resource 2). For simplicity, only results using global temperature as a trend term are given here. Using interaction terms in the regression did improve the R^2 results, but did not result in any additional significant models; in fact, for most islands there were fewer significant models (not shown). Both the full and additive models identified the same significant terms, and in the full models some of the interaction terms were found to be significant at the 95% level. Most of these significant interactions were in the E2 models (not shown), which is the EOF mode with the lowest correlations with the climate indices. For the dry season models, none of the interaction terms were significant for Hawai'i Island, while models for the other islands identified interaction terms with the PNAI—the index with almost no correlation with dry season rainfall. Due to the high similarities between the full and additive models, only results from the additive models are presented for the remainder of the paper.

The R^2 results from the additive models for all islands and seasons (Table 1) reveal that generally, the wet season had the best model fits (highest R^2 values) across all islands. For most islands and seasons, E1 had the best model fits, while the other components' results varied depending on the island and season. Based on the type II ANOVA results, the PNAI was the most significant term in almost all models (except in summer). The trend term was statistically significant only in the dry season (when PNAI was not a significant term) (Table 1). MEI was also significant only in dry season months. At the 95% level, the PDO index was significant for all E3 models in the wet season (except O'ahu), while in the dry season PDOI was significant only for E2 on Kaua'i and Maui.

Based on the percent variability explained by each EOF component (Fig. 6) and the R^2 results from the MLR models (Table 1), we calculated the amount of variability in rainfall that can be explained by ENSO, PDO, PNA, and global temperatures (anthropogenic trend term). For Kaua'i, the leading component E1 represents 84.2% of the total variance in the wet season, and the R^2 value for the wet season model containing MEI, PDOI, PNAI, and a trend term was 0.52. Therefore, about half (0.52) of the 84% of rainfall explained by E1 is accounted for by the four terms (MEI, PDOI, PNAI, trend). When the two are multiplied, 44% of winter rainfall

Table 1 P-values and R^2 values shown for the additive MLR models for the three leading EOF components (E1–E3) modeled as a combination of the three climate indices (MEI, PDOI, PNAI) and a trend term (global temperature) for each island and season

Nov–Apr							May–Oct						
		MEI	PDOI	PNAI	Trend	R^2			MEI	PDOI	PNAI	Trend	R^2
KA	E1	0.186	0.621	**0.000**	0.688	**0.52**	KA	E1	**0.012**	0.755	0.681	**0.009**	**0.18**
	E2	0.432	0.563	0.159	0.423	0.04		E2	**0.005**	**0.001**	0.561	0.856	**0.20**
	E3	0.668	**0.024**	0.207	0.057	**0.16**		E3	0.966	0.390	0.931	0.721	0.03
OA	E1	0.250	0.198	**0.000**	0.467	**0.40**	OA	E1	0.093	0.821	0.577	**0.045**	0.12
	E2	0.557	0.135	0.069	0.659	0.07		E2	0.500	0.259	0.280	0.632	0.05
	E3	0.203	0.401	0.255	0.488	0.06		E3	0.481	0.380	0.525	0.997	0.06
MA	E1	0.534	**0.029**	**0.000**	0.728	**0.34**	MA	E1	**0.017**	0.428	0.673	0.064	**0.21**
	E2	0.692	0.646	0.305	0.227	0.11		E2	0.294	**0.038**	0.749	0.641	0.09
	E3	0.113	**0.009**	0.097	0.338	**0.25**		E3	0.915	0.595	0.133	**0.020**	0.13
HA	E1	0.176	0.178	**0.001**	0.420	**0.39**	HA	E1	**0.006**	0.193	0.398	**0.000**	**0.35**
	E2	0.926	0.381	0.149	0.714	0.05		E2	0.911	0.569	0.514	**0.002**	**0.19**
	E3	0.123	**0.008**	0.232	0.680	**0.28**		E3	0.071	0.164	0.600	0.798	0.07

Bold values indicate $p < 0.05$. *KA* Kaua'i, *OA* O'ahu, *MA* Maui, *HA* Hawai'i Island

on Kaua'i, as represented by the first component (E1), is explained by ENSO, PDO, PNA, and global temperatures. On O'ahu, Maui and Hawai'i Island, 35%, 27% and 29% of wet season rainfall, respectively, can be explained by these three modes of natural variability and the trend term. The next two EOF components account for 0.5–2.3% on each island (maximum total (E1–E3) for wet season: 45% Kaua'i). For the dry season, a total of 16%, 10.4%, 15.7%, and 26.7% of summer rainfall can be explained by ENSO, PDO, PNA, and global temperatures on Kaua'i, O'ahu, Maui and Hawai'i Island, respectively. The remaining variability not explained by these factors is some combination of other natural and/or anthropogenic factors not represented by the climate indices or the trend term.

In summary, our task of identifying a trend contribution in the leading modes of rainfall variability gave mixed results. For the wet season, the interannual and decadal variability that is linked with PNA, ENSO, and PDO is too strong, such that trends cannot be distinguished in the relatively short data period from 1950 to 2012. In the dry season, when the direct influence from PNA and PDO is weaker, significant trends can be found influencing the overall spatiotemporal rainfall variability. The percent of explained variance is however small. These results suggest that the detection of secular trends in the 'temporal pattern' is limited by the low signal to noise (natural variability) ratio, and the shortness of the time series records. Alternatively, the next section explores an approach of detecting anthropogenically forced changes in the rainfall by means of spatial pattern analysis.

5.3 Pattern correlation coefficients

The downscaling patterns from both seasons and methods showed an overall windward/leeward split in the sign of the future trend patterns, with notable differences in the magnitude and spatial details between seasons and methods (Fig. 2). Any positive correlations in the PCC results (Fig. 10) indicate that the current trend patterns agree with the downscaling patterns in the sign of the trend, and stronger correlations indicate better spatial agreement. The PCC results for wet season and dry season show stronger correlations with the SDS maps than the DDS maps of future change in rainfall. PCCs with SDS and DDS maps in the wet season show negative correlations in the beginning of the historical data period, shifting to positive correlations toward the end of the record (2012). This result suggests that the observed winter trends are consistent with the anthropogenic forcing pattern that is expected to dominate the trends in future.

The dry season PCC results are more heterogeneous, with the sign of both the SDS and DDS correlations dependent on the time period considered. The PCCs in the most recent 20–30 years are strongly positive for SDS, and negative for DDS. The sign of the PCCs is generally opposite for SDS and DDS in the dry season. If the SDS future trend pattern was assumed to be correct, the strengthening of the spatial pattern correlation in the last 30 years would indicate that the recently observed trend pattern is part of the forced regional climate change response. If DDS was correct, the negative correlations in the last 30 years would indicate that the recent rainfall trends are mostly natural (unforced), and we would expect the trend pattern to change in the coming decades to match the DDS pattern.

6 Discussion

The EOF analysis performed on seasonal gridded rainfall data for the State of Hawai'i revealed that more variability was explained in the wet season than in the dry

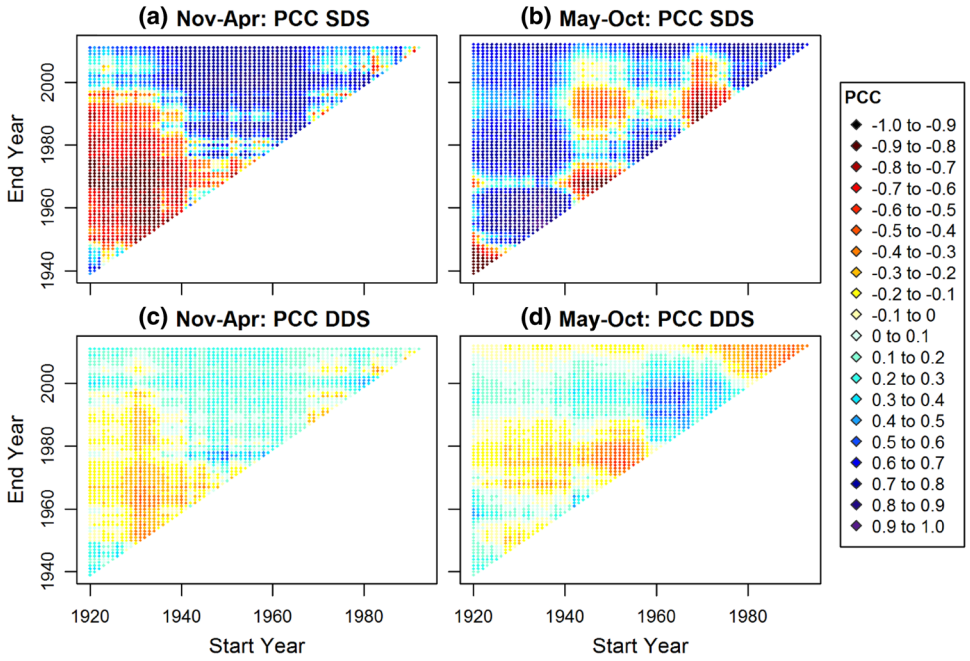

Fig. 10 Pattern correlation coefficients (PCC) between all possible rainfall trend maps between 1920 and 2012 (including 20 years or more) and future expected change in rainfall (downscaling results). PCC with statistical downscaling (SDS) results for 2071–2100 from CMIP5 RCP8.5 scenario for wet season (Nov.-Apr.) (**a**) and dry season (May-Oct.) (**b**) and PCC with dynamical downscaling (DDS) results for 2080–2099 from CMIP3 A1B scenario for wet season (**c**) and dry season (**d**)

season. The highest variation explained was found in the first component (E1) in the wet season, when the majority of annual rainfall occurs for most places in Hawai'i. Dry season months have proven difficult for statistical methods in Hawai'i. The SDS method, for example, had difficulty linking station rainfall with large-scale seasonal mean circulation in the dry season, with lower correlations and poorer downscaling skill than in the wet season (Timm and Diaz 2009; Elison Timm et al. 2015). The limited ability to capture small-scale and infrequent rain-producing disturbances leads to lower confidence in dry season SDS results, and could explain the noisy PCC results (Fig. 10). The SDS projections indicate that some leeward areas will experience up to 90% decreases, a value that must be considered with caution due to the limits of linear statistical downscaling methods. DDS projections show increases of up to 60% in windward areas, including 30% wetter conditions at the wettest spot in Hawai'i known as Big Bog on Maui, which already receives an average of over 10,000 mm annually (Giambelluca et al. 2013). Based on the recent trends observed in the dry season, either both the SDS and DDS dry season maps are unrealistic, or the observed trend was mostly an unforced signal and future trends would likely show a different signature resembling one of the downscaled maps. The large discrepancies in the strength of the pattern correlations with the future percent change maps in both seasons imply that the recent rainfall trend patterns are better captured by the SDS method than the DDS method. It should be noted that the SDS results use the latest global model projections (CMIP5) and the emissions scenarios are defined differently than the CMIP3 scenarios, so differences in PCC results between SDS and DDS in this case could be due to different input models and scenario choices. Nonetheless, a general agreement in the pattern correlations of future rainfall and the observed trends in the second half of the twentieth century suggest that a forced contribution to the observed winter trends is likely. However, the temporal trend analysis with the MLR failed to detect a significant trend contribution.

In the multiple regression analysis, PNAI was the dominant term in the wet season. PNAI was significant for E1 on every island in the wet season (Table 1), and had higher correlations with the leading components than MEI or PDOI (Fig. 9). Based on the initial correlation analysis between PNAI and rainfall (Fig. 4), the high correlations with the EOFs are not surprising. MEI and PDOI did not exhibit a strong influence on most models in the wet season; the influence of the extratropical atmosphere on rainfall in Hawai'i is best represented by the PNA index. One should point out that in the MLR the dominant predictor can diminish the relative importance of the other predictors (due to multicollinearity). The influence of tropical Pacific ENSO variability on the extratropical atmosphere is of course not disputed here. The PNAI measures the ENSO-induced circulation teleconnection as well as the internally 'weather generated' extratropical variability of the Aleutian Low, storm tracks, and the strength and position of the subtropical high. Most studies in Hawai'i that discuss natural climate variability focus on ENSO and PDO as the dominant modes, and PNA is often ignored. The PNA phases result in 500 hPa geopotential height anomalies directly over the Hawaiian Islands, meaning this low-frequency mode of variability has

the most direct influence on Hawai'i's winter rainfall (compared to ENSO and PDO).

Although the three modes of natural climate variability significantly contributed to several of the MLR models, many islands and seasons had no significant regression model results. For example, E2 in the wet season had no significant terms on any island and very low R^2 values (Table 1). This indicates that a large amount of the total variability is still not accounted for by these natural modes of variability and the trend term. Even for the island and season with the highest amount of variability explained by the leading EOF modes, the linear regression models only explain less than 45% of the total variability (E1-E3, Nov.–Apr. on Kaua'i). The remaining variability is likely a result of a combination of other modes of natural climate variability and local factors. Additional work is needed to identify these local factors and other modes of variability to assess their influence on secular rainfall changes. The trade wind inversion (TWI), for example, is an important factor known to influence rainfall across the state and has seen an increased frequency of occurrence since 1990, leading to drying at high elevations (Longman et al. 2015). Identifying the dominant factors is especially important in summer months, where these large-scale modes of climate variability have weaker signals, and only a small percent of the total variability can be explained. Better understanding the drivers of summer rainfall in Hawai'i would benefit future downscaling and modeling efforts.

To address whether a detectable anthropogenic influence on rainfall has been found in Hawai'i, two lines of evidence were used: whether the trend term was significant in the MLR models, and whether the PCC results showed strong positive correlations between recent trends and the expected future change (utilizing the SDS and DDS projections). The dry season was the only season where the trend term in the MLR was consistently significant across the islands, however the R^2 values for most of these models were low. In the wet season, the trend term was not significant in any models, indicating that the terms representing natural variability were dominant compared to the anthropogenic trend term in this season. We interpret these results as an absence of (or weak) anthropogenic trend signal in the observed wet season rainfall time series. It should be noted that the EOF analysis itself may remove or reduce the trend signal in the presence of strong covariations induced by natural modes of variability (Elison Timm et al. 2016). In such cases the EOF truncation could affect the MLR trend analysis results. However, the leading components (E1–E3) reproduced the observed trend pattern reasonably well ($r = 0.71$, O'ahu dry season, not shown). Thus, a trend component should become detectable in the leading EOF modes when the signal amplitude emerges from the background variability. For the wet season, however, the observed trend pattern is not well represented in the low-dimensional subspace of the three leading EOF patterns ($r = 0.24$, O'ahu wet season, not shown).

The spatial patterns of recent trends in the dry season did not resemble the expected patterns of future change (inconsistent PCCs, Fig. 10b, d). The trend patterns from the most recent 30 years in the SDS comparison may point to some strong agreement with future patterns (Fig. 10b), but other periods in the record also had high positive correlations and these fluctuated through time. The wet season PCC results (Fig. 10a, c), however, show that recent rainfall trends that include the latter part of the period are positively correlated with future expected changes in rainfall as projected by SDS and DDS, which can be interpreted as an anthropogenic contribution to the recently observed trends. These PCC results in winter show the pattern we would expect if an anthropogenic signal were emerging. However, given these conflicting lines of evidence in both seasons from both methods, it is not possible to conclude with certainty that a detectable anthropogenic signal has emerged above natural variability in Hawaiian rainfall at this time.

One has to remember that this statistical detection method (and other similar observation-based methods) cannot provide conclusive statements with regards to the attribution to anthropogenic forcing. It has to be acknowledged that the instrumental data period does not provide sufficient data to estimate the modes of natural variability in the pre-industrial era. Without that background information, a formal attribution of twentieth century trends remains ambiguous - even if highly significant trends were detected. One possible solution would be to simulate the pre-industrial rainfall variability with well-validated regional climate models. However, given the small spatial extent of Hawai'i, attempting formal attribution techniques with the aid of regional climate models is difficult. Although these methods would allow simulations of rainfall with and without anthropogenic forcings and provide a more conclusive answer, they would still face problems attempting to reconcile the small-scale factors that influence rainfall. As the technology improves and computing time is reduced, more simulations of high resolution rainfall will be possible and in the future we hope to be able to conclusively determine whether anthropogenic forcings have impacted rainfall in Hawai'i. The empirical methods described here provide a first attempt to describe the influences on secular rainfall variations in Hawai'i, and underscore the difficulties involved in regional attribution studies. We advocate that regional downscaling efforts should concentrate not only on the future climate, but equal, perhaps greater priority should be given to the downscaling of control or pre-industrial climate variability in order to improve the formal detection and attribution of regionally observed climate changes.

Acknowledgements We like to thank the anonymous reviewers for their constructive feedback and the critical review the manuscript. This work is supported by the US Army Corps of Engineers Honolulu District, the Hawai'i Commission on Water Resource Management, Pacific RISA, and Pacific Islands Climate Science Center (PICSC). We would also like to thank Ryan Longman, Heidi Needham, Mami Takahashi-LeMaster, Yoshiyuki Miyazawa, Shelley Crausbay, Creighton Litton, and Camilo Mora for discussions, support, technical support, and review of earlier drafts.

References

Ashcroft L, Karoly DJ, Gergis J (2014) Southeastern Australian climate variability 1860–2009: a multivariate analysis. Int J Climatol 34:1928–1944. https://doi.org/10.1002/joc.3812

Barnston AG, Livezey RE (1987) Classification, seasonality and persistence of low-frequency atmospheric circulation patterns. Mon Weather Rev 115:1083–1126

Bhend J, von Storch H (2008) Consistency of observed winter precipitation trends in northern Europe with regional climate change projections. Clim Dyn 31:17–28. https://doi.org/10.1007/s00382-007-0335-9

Brunetti M, Caloiero T, Coscarelli R et al (2012) Precipitation variability and change in the Calabria region (Italy) from a high resolution daily dataset. Int J Climatol 32:57–73. https://doi.org/10.1002/joc.2233

Cao G, Giambelluca TW, Stevens DE, Schroeder TA (2007) Inversion variability in the Hawaiian trade wind regime. J Clim 20:1145–1160. https://doi.org/10.1175/JCLI4033.1

Chen WY, Van den Dool H (2003) Sensitivity of teleconnection patterns to the sign of their primary action center. Mon Weather Rev 131:2885–2899

Chu P-S, Chen H (2005) Interannual and interdecadal rainfall variations in the Hawaiian Islands. J Clim 18:4796–4813. https://doi.org/10.1175/JCLI3578.1

Chu P-S, Nash AJ, Porter F-Y (1993) Diagnostic studies of two contrasting rainfall episodes in Hawaii: dry 1981 and wet 1982. J Clim 6:1457–1462

Chu PS, Chen YR, Schroeder TA (2010) Changes in precipitation extremes in the Hawaiian Islands in a warming climate. J Clim 23:4881–4900. https://doi.org/10.1175/2010JCLI3484.1

Chylek P, Dubey MK, Lesins G et al (2014) Imprint of the Atlantic multi-decadal oscillation and Pacific decadal oscillation on southwestern US climate: Past, present, and future. Clim Dyn 43:119–129. https://doi.org/10.1007/s00382-013-1933-3

Diaz HF, Giambelluca TW (2012) Changes in atmospheric circulation patterns associated with high and low rainfall regimes in the Hawaiian Islands region on multiple time scales. Glob Planet Change 98–99:97–108. https://doi.org/10.1016/j.gloplacha.2012.08.011

Elison Timm O, Diaz HF, Giambelluca TW, Takahashi M (2011) Projection of changes in the frequency of heavy rain events over Hawaii based on leading Pacific climate modes. J Geophys Res Atmos 116:1–12. https://doi.org/10.1029/2010JD014923

Elison Timm O, Giambelluca TW, Diaz HF (2015) Statistical downscaling of rainfall changes in Hawai'i based on the CMIP5 global model projections. J Geophys Res Atmos 120:92–112. https://doi.org/10.1002/2014JD022059

Elison Timm O, Flamholtz W, Li S et al (2016) Testing the Reconstruction Potential for North Pacific Circulation Anomalies inside the TraCE-21 ka Paleoclimate Simulation. AGU Fall Meeting. San Francisco, CA

Elsanabary MH, Gan TY, Mwale D (2014) Application of wavelet empirical orthogonal function analysis to investigate the nonstationary character of Ethiopian rainfall and its teleconnection to nonstationary global sea surface temperature variations for 1900–1998. Int J Climatol 34:1798–1813. https://doi.org/10.1002/joc.3802

Feng J, Li J (2011) Influence of El Niño Modoki on spring rainfall over south China. J Geophys Res Atmos 116:1–10. https://doi.org/10.1029/2010JD015160

Frazier AG, Giambelluca TW (2017) Spatial trend analysis of Hawaiian rainfall from 1920 to 2012. Int J Climatol 37:2522–2531. https://doi.org/10.1002/joc.4862

Frazier AG, Giambelluca TW, Diaz HF, Needham HL (2016) Comparison of geostatistical approaches to spatially interpolate month-year rainfall for the Hawaiian Islands. Int J Climatol 36:1459–1470. https://doi.org/10.1002/joc.4437

Giambelluca TW, Chen Q, Frazier AG et al (2013) Online Rainfall Atlas of Hawai'I. Bull Am Meteorol Soc 94:313–316. https://doi.org/10.1175/BAMS-D-11-00228.1

Hamlington BD, Leben RR, Strassburg MW et al (2013) Contribution of the Pacific Decadal Oscillation to global mean sea level trends. Geophys Res Lett 40:5171–5175. https://doi.org/10.1002/grl.50950

Hannachi A, Jolliffe IT, Stephenson DB (2007) Empirical orthogonal functions and related techniques in atmospheric science: A review. Int J Climatol 27:1119–1152. https://doi.org/10.1002/joc.1499

Hegerl G, Zwiers F (2011) Use of models in detection and attribution of climate change. Wiley Interdiscip Rev Clim Chang 2:570–591. https://doi.org/10.1002/wcc.121

Hoerling M, Hurrell J, Eischeid J, Phillips A (2006) Detection and attribution of twentieth-century northern and southern African rainfall change. J Clim 19:3989–4008. doi: https://doi.org/10.1175/JCLI3842.1

Juvik SP, Juvik JO (1998) Atlas of Hawai'i. University of Hawai'i Press, Honolulu

Kim BH, Ha KJ (2015) Observed changes of global and western Pacific precipitation associated with global warming SST mode and mega-ENSO SST mode. Clim Dyn 45:3067–3075. https://doi.org/10.1007/s00382-015-2524-2

Kolker AS, Hameed S (2007) Meteorologically driven trends in sea level rise. Geophys Res Lett 34:1–7. https://doi.org/10.1029/2007GL031814

Kruk MC, Lorrey AM, Griffiths GM et al (2015) On the state of the knowledge of rainfall extremes in the western and northern Pacific basin. Int J Climatol 35:321–336. https://doi.org/10.1002/joc.3990

Krushelnycky PD, Loope LL, Giambelluca TW et al (2013) Climate-associated population declines reverse recovery and threaten future of an iconic high-elevation plant. Glob Chang Biol 19:911–922. https://doi.org/10.1111/gcb.12111

Krushelnycky PD, Starr F, Starr K et al (2016) Change in trade wind inversion frequency implicated in the decline of an alpine plant. Clim Chang Responses 3:1. https://doi.org/10.1186/s40665-016-0015-2

L'Heureux ML (2004) Atmospheric circulation influences on seasonal precipitation patterns in Alaska during the latter 20th century. J Geophys Res 109:1–17. https://doi.org/10.1029/2003JD003845

Lauer A, Zhang C, Elison-Timm O et al (2013) Downscaling of climate change in the hawaii region using CMIP5 results: On the choice of the forcing fields*. J Clim 26:10006–10030. https://doi.org/10.1175/JCLI-D-13-00126.1

Longman RJ, Diaz HF, Giambelluca TW (2015) Sustained increases in lower-tropospheric subsidence over the Central Tropical North Pacific drive a decline in high-elevation rainfall in Hawaii. J Clim 28:8743–8759. https://doi.org/10.1175/JCLI-D-15-0006.1

Lyons SW (1982) Empirical orthogonal function analysis of Hawaiian rainfall. J Appl Meteorol 21:1713–1729

Mantua NJ, Hare SR (2002) The Pacific Decadal Oscillation. J Oceanogr 58:35–44

Mantua NJ, Hare SR, Zhang Y et al (1997) A Pacific interdecadal climate oscillation with impacts on salmon production. Bull Am Meteorol Soc 78:1069–1079

Meyssignac B, Salas Y, Melia D, Becker M et al (2012) Tropical Pacific spatial trend patterns in observed sea level: Internal variability and/or anthropogenic. signature? Clim Past 8:787–802. https://doi.org/10.5194/cp-8-787-2012

Newman M, Alexander MA, Ault TR et al (2016) The Pacific Decadal Oscillation, Revisited. J Clim 29:4399–4427. https://doi.org/10.1175/JCLI-D-15-0508.1

Ning L, Bradley R (2014) Winter precipitation variability and corresponding teleconnections over the northeastern United States. J Geophys Res 119:7931–7945. https://doi.org/10.1002/2014JD021591.Received

Noake K, Polson D, Hegerl G, Zhang X (2012) Changes in seasonal land precipitation during the latter twentieth-century. Geophys Res Lett 39:1–5. https://doi.org/10.1029/2011GL050405

North GR, Bell TL, Cahalan RF (1982) Sampling errors in the estimation of empirical orthogonal funtions. Mon Weather Rev 110:699–706

O'Connor CF, Chu PS, Hsu PC, Kodama K (2015) Variability of Hawaiian winter rainfall during La Niña events since 1956. J Clim 28:7809–7823. https://doi.org/10.1175/JCLI-D-14-00638.1

Sarojini BB, Stott PA, Black E (2016) Detection and attribution of human influence on regional precipitation. Nat Clim Chang 6:669–675. https://doi.org/10.1038/nclimate2976

Silvestri GE, Vera CS (2003) Antarctic oscillation signal on precipitation anomalies over southeastern South America. Geophys Res Lett 30:1–4. https://doi.org/10.1029/2003GL018277

Stott PA, Tett SF (1998) Scale-dependent detection of climate change. J Clim 11(12):3282–3294. https://doi.org/10.1175/1520-0442(1998)011<3282:SDDOCC>2.0.CO;2

Stott PA, Gillett NP, Hegerl GC et al (2010) Detection and attribution of climate change: A regional perspective. Wiley Interdiscip Rev Clim Chang 1:192–211. https://doi.org/10.1002/wcc.34

Taschetto AS, England MH (2009) El Niño Modoki impacts on Australian rainfall. J Clim 22:3167–3174. https://doi.org/10.1175/2008JCLI2589.1

Timm O, Diaz HF (2009) Synoptic-statistical approach to regional downscaling of IPCC twenty-first-century climate projections: Seasonal rainfall over the Hawaiian Islands. J Clim 22:4261–4280. https://doi.org/10.1175/2009JCLI2833.1

Ummenhofer CC, Sen Gupta A, England MH (2009) Causes of late twentieth-century trends in New Zealand precipitation. J Clim 22:3–19. https://doi.org/10.1175/2008JCLI2323.1

Van Den Dool HM, Saha S, Johansson A (2000) Empirical orthogonal teleconnections. J Clim 13:1421–1435. https://doi.org/10.1175/1520-0442(2000)013<1421:EOT>2.0.CO;2

Wallace JM, Gutzler DS (1981) Teleconnections in the Geopotential Height Field during the Northern Hemisphere Winter. Mon Weather Rev 109:784–812

Wang H, Schubert S, Suarez M et al (2009) Attribution of the seasonality and regionality in climate trends over the United States during 1950–2000. J Clim 22:2571–2590. https://doi.org/10.1175/2008JCLI2359.1

Wolter K, Timlin MS (2011) El Niño/Southern Oscillation behaviour since 1871 as diagnosed in an extended multivariate ENSO index (MEI.ext). Int J Climatol 31:1074–1087. https://doi.org/10.1002/joc.2336

Xiao M, Zhang Q, Singh VP (2015) Influences of ENSO, NAO, IOD and PDO on seasonal precipitation regimes in the Yangtze River basin, China. Int J Climatol 35:3556–3567. doi: https://doi.org/10.1002/joc.4228

Zhang X, Zwiers FW, Hegerl GC et al (2007) Detection of human influence on twentieth-century precipitation trends. Nature 448:461–465. https://doi.org/10.1038/nature06025

Zhang C, Wang Y, Hamilton K, Lauer A (2016a) Dynamical downscaling of the climate for the Hawaiian Islands. Part I: present day. J Clim 29:3027–3048. https://doi.org/10.1175/JCLI-D-15-0432.1

Zhang C, Wang Y, Hamilton K, Lauer A (2016b) Dynamical downscaling of the climate for the Hawaiian islands. Part II: Projection for the late twenty-first century. J Clim 29:8333–8354. https://doi.org/10.1175/JCLI-D-16-0038.1